SARS-CoV-2 variants do not evolve to promote further escape from MHC-I recognition

Miyu Moriyama[1], Carolina Lucas[1], Valter Silva Monteiro[1], and Akiko Iwasaki[1,2,3]

[1]Department of Immunobiology, Yale School of Medicine, New Haven, CT 06519, USA.

[2]Department of Molecular Cellular and Developmental Biology, Yale University, New Haven CT 06520, USA.

[3]Howard Hughes Medical Institute, Chevy Chase, MD 20815, USA.

Key words: CD8 T cell; cytotoxic T cell; MHC; viral evasion; COVID-19; variants of concern; respiratory viruses

Summary

SARS-CoV-2 variants of concern (VOCs) possess mutations that confer resistance to neutralizing antibodies within the Spike protein and are associated with breakthrough infection and reinfection. By contrast, less is known about the escape from $CD8^+$ T cell-mediated immunity by VOC. Here, we demonstrated that VOCs retain similar MHC-I downregulation capacity compared to the ancestral virus. However, VOCs exhibit a greater ability to suppress type I IFN than the ancestral virus. Although VOCs possess unique mutations within the ORF8 gene, which suppresses MHC-I expression, none of these mutations enhanced the ability of ORF8 to suppress MHC-I expression. Notably, MHC-I upregulation was strongly inhibited after the ancestral SARS-CoV-2 infection *in vivo*. Collectively, our data suggest that the ancestral SARS-CoV-2 already possesses an intrinsically potent MHC-I evasion capacity, and that further adaptation by the variants was not observed.

Introduction

SARS-CoV-2 has continued to evolve since it was first detected in Wuhan, China in December 2019. Beginning in late 2020, a number of SARS-CoV-2 variants with increased transmissibility, immune evasion capacity, and pathogenicity, which are known as variants of concern (VOCs) and variants of interest (VOIs) have emerged. Increasing breakthrough infection and reinfection events were associated with the emergence of VOCs (Kustin et al., 2021; Tao et al., 2021). Breakthrough infections and reinfections are likely driven by the significant increase in transmissibility (Sabino et al., 2021), evasion from innate immunity (Guo et al., 2021; Thorne et al., 2022), and escape from the neutralization by vaccine/infection-induced antibodies against VOCs (Garcia-Beltran et al., 2021; Lucas et al., 2021; Planas et al., 2022; Wang et al., 2021). By contrast, minimal evasion of T cell epitopes has been reported for VOCs (Tarke et al., 2021b).

$CD8^+$ cytotoxic T lymphocyte (CTL) recognizes and kills infected cells and eliminates the source of replicating viruses. Antigen presentation by major histocompatibility complex class I (MHC-I) is a critical step for activation of antigen-specific $CD8^+$ T cells and subsequent killing of infected cells. Viral

peptides processed by the cellular proteasome complex are loaded on MHC-I molecule in the endoplasmic reticulum and translocate to the cell surface to be recognized by antigen-specific $CD8^+$ T cells. To successfully establish infection and replicate in the host, many viruses have acquired the ability to inhibit MHC-I processing and presentation of viral antigens (Hansen and Bouvier, 2009). Likewise, SARS-CoV-2 utilizes its viral proteins to interfere with the MHC-I pathway (Yoo et al., 2021; Zhang et al., 2021). SARS-CoV-2 ORF8 protein induces autophagic degradation of MHC-I and confers resistance to CTL surveillance (Zhang et al., 2021). Studies from the first 3 months of the pandemic showed the rapid evolution of the SARS-CoV-2 ORF8 gene including isolates with 382nt deletion spanning ORF7b-ORF8 gene region (Su et al., 2020; Velazquez-Salinas et al., 2020), which is associated with robust T cell response and mild clinical outcome (Fong et al., 2022; Young et al., 2020). These findings collectively raised a question of whether VOC and its ORF8 protein have evolved to further enhance the ability to shut down MHC-I, thereby evading from antigen-specific memory $CD8^+$ T cells established by previous infection or vaccination.

Here, we performed a systematic analysis of the capacity of SARS-CoV-2 variants to downregulate MHC-I presentation. Our data unexpectedly

demonstrated vigorous suppression of MHC-I system by the ancestral SARS-CoV-2 virus and minimal evolution in modulating MHC-I pathway by VOCs.

Results

SARS-CoV-2 variants retain similar MHC-I evasion capacity

To investigate the impact of SARS-CoV-2 infection on MHC-I expression, we infected Calu-3 cells, a commonly used human lung epithelial cell line, with SARS-CoV-2 variants and the ancestral strain (USA-WA1). We tested four variants of concern (B.1.1.7/Alpha, B.1.351/Beta, P.1/Gamma, and B.1.617.2/Delta) and three variants of interest (B.1.427/Epsilon, B.1.429/Epsilon, and B.1.526/Iota). SARS-CoV-2 variants and the ancestral strain similarly downregulated MHC-I levels after infection (Fig.1A). We next examined transcriptional levels of MHC-I genes after infection with SARS-CoV-2 variants. Transcriptional levels of MHC-I genes differed depending on the variants (Fig.1B). The ancestral strain significantly downregulated HLA-A, B, and C genes as previously reported (Yoo et al., 2021). B.1.1.7 and B.1.351 showed a similar reduction in HLA-A, B, and C mRNA expression as the ancestral strain. Other variants showed a weaker downregulation (B.1.526), no significant change (B.1.429), or upregulation (P.1) of HLA class I genes within the infected cells. These results indicated that SARS-CoV-2 variants maintain similar capacity to reduce HLA transcription as the ancestral virus, except for the P.1 and B.1.429

variants. Given that P.1-infected and B.1.429-infected cells still expressed low levels of MHC-I on the surface, other genes involved in the MHC-I processing and presentation pathway, many of which are ISGs, may be dampened by the infection.

Variant-specific mutations are found in ORF8 gene of SARS-CoV-2

We next performed multiple sequence alignment of ORF8 protein sequences from SARS-CoV-2 variants to see if there are any non-synonymous mutations. In total, 7 non-synonymous mutations and 2 deletions are detected from 10 variants examined (Fig. S1). Notably, a premature stop codon was introduced at Q27 of B.1.1.7, which truncates the ORF8 polypeptide length and likely alters the protein functionality. The downstream mutations (R52I and Y73C) probably have no further impact on B.1.1.7 ORF8 protein because of the early translation termination by Q27stop mutation. In addition to B.1.1.7/Alpha, all other variants of concern (B.1.351/Beta, P.1/Gamma, and B.1.617.2/Delta) harbored mutations or deletions in ORF8 protein except for BA.1/Omicron variant. Two of the former variants of interest, B.1.429/Epsilon and B.1.526/Iota harbored V100L and T11I mutation respectively. None of the mutations and deletions were

conserved among different lineages. To investigate the prevalence of mutations found in variants, we downloaded 3,059 SARS-CoV-2 genome sequence data from GISAID database (https://www.gisaid.org/). We found that the mutation in a particular amino acid is only exclusively seen in a single lineage (Fig.2A). ORF8 L84S mutation, which was detected within the first 2 months of pandemic (Ceraolo and Giorgi, 2020) and corresponding to clade S, was not observed in any of the variants. We also observed the mutations discovered by multiple sequence alignment are generally highly prevalent, and the proportions ranged from 12.5 to 100% of the lineage (Fig.2B). These results indicate that the variant-specific mutations were acquired independently during SARS-CoV-2 evolution.

Impaired MHC-I downregulation by B.1.1.7 ORF8 protein

We next tested whether variant-specific mutations alter MHC-I downregulating capability of ORF8 protein. To this end, we generated expression plasmids encoding six ORF8 mutants from SARS-CoV-2 variants (Fig.2C), and subsequently transfected HEK293T cells with these plasmids for the detection of its effect on the surface MHC-I expression levels. We included SARS-CoV ORF8a/b proteins as negative controls, as they have been shown not to affect

MHC-I expression levels (Zhang et al., 2021). Since ORF8 induces degradation of MHC-I via autophagy by interacting with MHC-I and localizing in LC3-positive puncta (Zhang et al., 2021), ORF8 presumably acts on MHC-I downregulation in cell-intrinsic manner. Indeed, surface MHC-I levels of the cells expressing WT ORF8 protein were much lower than those of the cells without ORF8 expression (Fig.2D). Among six ORF8 mutants tested, five mutants including I121L, E92K, del119-120, V100L, and T11I downregulated surface MHC-I levels of the cells expressing those proteins to a similar extent to WT ORF8 protein did (Fig.2E). On the other hand, Q27Stop ORF8 mutant showed significantly attenuated MHC-I downregulation capability compared to the WT ORF8 protein. These results indicated that none of the variant-specific mutations enhanced the ability of ORF8 protein to downregulate MHC-I, and the ORF8 encoded by the B.1.1.7 lineage was attenuated in its ability to reduce surface MHC I expression.

SARS-CoV-2 variants acquire an enhanced IFN evasion capacity

Given that B.1.1.7 and P.1 variants were able to reduce MHC-I expression levels even though these lineages retain functionally defective ORF8 mutant or are less effective in reducing HLA-I mRNA levels, we examined whether SARS-

CoV-2 variants suppress interferon-stimulated gene (ISG) induction more strongly than the ancestral strain. Interestingly, all variants tested significantly reduced upregulation of ISG expressions compared to the ancestral strain (Fig.3). These results indicated that SARS-CoV-2 variants have an increased capacity to suppress ISGs, which may include genes involved in MHC I processing and presentation pathways.

Multiple SARS-CoV-2 viral proteins play redundant roles in the downregulation of MHC-I

As another possible compensation mechanism, we investigated the possibility that SARS-CoV-2 encodes multiple viral genes that redundantly act on MHC-I downregulation. We generated expression plasmids encoding SARS-CoV-2 E, M, ORF7a, and ORF7b, and assessed the effect on the surface MHC-I and MHC-II expression levels of HEK293T cells following transfection with these plasmids. We also included Human Immunodeficiency Virus (HIV) Nef as a positive control for downregulating both MHC-I and MHC-II (Schwartz et al., 1996; Stumptner-Cuvelette et al., 2001), and SARS-CoV ORF8a/b proteins as a negative control. As expected, HIV Nef protein downregulated both MHC-I and

MHC-II levels, whereas SARS-CoV-2 ORF8 specifically targeted MHC-I (Fig.4A-B). We found that in addition to ORF8, SARS-CoV-2 E, M, and ORF7a substantially downregulated MHC-I within the cells expressing these viral proteins (Fig. 4C). Significant reduction of surface MHC-II levels was also observed by expression of these viral proteins (Fig. 4C), albeit to a lesser extent (~20%). These results suggested that SARS-CoV-2 encodes multiple viral genes that are redundantly downregulating MHC-I likely to ensure viral evasion from MHC-I-mediated CTL recognition.

Superior MHC-I evasion by SARS-CoV-2 compared to influenza A virus *in vivo*

In the experiments above, we have shown that SARS-CoV-2 encodes multiple viral proteins that are targeting MHC-I expression, which can synergistically strengthen the capability of the virus to avoid MHC-I presentation. We also demonstrated that SARS-CoV-2 variants have an enhanced capacity to suppress ISG induction than the ancestral strain but not MHC-I, which raised the possibility that the MHC-I evasion strategy was already optimal in the ancestral strain. Moreover, we confirmed the previous finding that the MHC-I

downregulation is a newly acquired function of SARS-CoV-2 ORF8 protein, which was not seen in SARS-CoV ORF8a/b proteins. Considering these results, we hypothesized that even the ancestral strain of SARS-CoV-2 possesses a superior MHC-I evasion strategy than other respiratory viruses. To assess this hypothesis, we infected C57BL/6J mice intranasally with a mouse-adapted strain of SARS-CoV-2 (SARS-CoV-2 MA10) or influenza A/PR8 virus and analyzed the MHC-I expression levels of lung epithelial cells at 2 days after infection. SARS-CoV-2 MA10 virus harbors 2 mutations in the Spike protein, 3 mutations in the ORF1ab, and an F7S mutation in ORF6 compared to the ancestral virus (Leist et al., 2020). Strikingly, influenza A virus induced robust upregulation of MHC-I in both infected (NP+) and uninfected (NP-) lung epithelial cells, whereas SARS-CoV-2 MA10 upregulated MHC-I only in uninfected cells (S-), and to a lesser extent than the influenza virus (Fig.5A-C). Importantly, MHC-I upregulation was completely blocked in SARS-CoV-2 MA10 infected (S+) lung epithelial cells, suggesting that SARS-CoV-2 viral proteins are strongly inhibiting MHC-I upregulation in a cell-intrinsic manner. These results indicated that SARS-CoV-2 possesses a near complete ability to shut down MHC-I induction within infected cells in vivo, a feature not found in influenza A virus.

Discussion

$CD8^+$ T cell-mediated elimination of infected cells plays an important role in the antiviral adaptive immune response. Thus, many viruses have developed ways to avoid the efficient MHC-I mediated antigen presentation to $CD8^+$ T cells. In the current study, we uncovered the intrinsically potent ability of SARS-CoV-2 to shut down the host MHC-I system by using live, authentic SARS-CoV-2 variants as well as the functional analysis of variant-specific mutations in ORF8 gene, a key viral protein for both MHC-I evasion and adaptation to the host.

We demonstrated that most variants of concern/interest possess unique mutations within ORF8 gene. By functional analysis using mutant ORF8, we found that none of the mutations enhanced the ability of ORF8 to suppress MHC-I presentation. Rather, the mutation in B.1.1.7/Alpha lineage attenuated its function. These results raised the question if these mutations are beneficial for the virus. One possibility is that these mutations play roles in modifying ORF8 functions independent of MHC-I downregulation. Our data indeed demonstrated the enhanced ability of VOCs to suppress ISG expression. Multiple functions of SARS-CoV-2 ORF8 were reported so far, which include inhibition of type I IFN, ISGs, or NF-kB signaling (Geng et al., 2021; Lei et al., 2020; Li et al., 2020) and

modulation of cytokine expression from macrophages (Kriplani et al., 2021). Interestingly, several studies showed that SARS-CoV-2 ORF8 is actively secreted into the cell culture media in a signal peptide-dependent manner when it is overexpressed *in vitro* (Kriplani et al., 2021; Wang et al., 2020). Furthermore, ORF8 peptides and anti-ORF8 antibodies can be detected abundantly in serum of patients, suggesting the relevance of the active secretion of ORF8 to actual infection in humans (Wang et al., 2020).

ORF8 is implicated in adaptation to the human host during the SARS-CoV outbreak (Chinese SARS Molecular Epidemiology Consortium, 2004; Guan et al., 2003), and it is known that ORF8 is the hypervariable genomic region among the SARS-CoV and bat SARS-related CoVs (Cui et al., 2019; Hu et al., 2017). Likewise, studies from early in the COVID-19 pandemic observed the variability and rapid evolution of SARS-CoV-2 ORF8 gene (Alkhansa et al., 2021; Velazquez-Salinas et al., 2020). Notably, SARS-CoV-2 isolates with 382nt deletion spanning ORF7b-ORF8 gene region were observed in Singapore (Su et al., 2020), which correlated with robust T cell response and mild clinical outcome (Fong et al., 2022; Young et al., 2020). Mutations in ORF8 gene thus may play a key role in modulating viral pathogenesis and adaptation to the host by regulating

MHC-I levels and ISGs.

The enhanced immune evasion by VOCs has been well documented for escape from neutralizing antibodies (Garcia-Beltran et al., 2021; Lucas et al., 2021; Planas et al., 2022; Wang et al., 2021) and from innate immune responses (Guo et al., 2021; Thorne et al., 2022). Here we demonstrated that SARS-CoV-2 variants of concern have evolved to better limit the host type I IFN response. In contrast, the ability to reduce MHC-I expression remained unchanged throughout VOC evolution. These findings suggested two important perspectives on the MHC-I evasion strategy of SARS-CoV-2. First, SARS-CoV-2 utilizes multiple redundant strategies to suppress MHC-I expression. For example, considering B.1.1.7 retained an intact ability to shut down MHC-I, the impaired MHC-I evasion by B.1.1.7 ORF8 is likely compensated by the redundant and/or compensatory functions of other viral proteins including E, M, and ORF7a. In addition, B.1.1.7 lineage has been shown to express an increased subgenomic RNA and protein abundance of ORF6 (Thorne et al., 2022), which suppresses MHC-I at the transcriptional level by interfering with STAT1-IRF1-NLRC5 axis (Yoo et al., 2021). The multi-tiered MHC-I evasion mechanisms thus work redundantly to ensure escape from CTL killing.

Second, MHC-I downregulation may not only impair CTL recognition of infected cells for killing but may also impair priming of CD8 T cells. Indeed, the frequency of circulating SARS-CoV-2 specific memory $CD8^+$ T cells in SARS-CoV-2 infected individuals are ~10 fold lower than for influenza or Epstein-Barr virus-specific T cell populations (Habel et al., 2020), which indicates the suboptimal induction of memory $CD8^+$ T cells following SARS-CoV-2 infection in human.

Third, given that the variants of concern had not further evolved to downregulate MHC-I more strongly than the original strain, SARS-CoV-2 ancestral virus was already fully optimized for escape from $CD8^+$ T cell-mediated immunity with respect to downregulation of MHC-I expression and is under no evolutionary pressure to further optimize the evasion strategy. However, mutations and evasion from particular HLA-restricted CTL epitopes have been observed in circulating SARS-CoV-2 and VOCs (Agerer et al., 2021; Motozono et al., 2021). Genome-wide screening of epitopes suggested the $CD8^+$ T and $CD4^+$ T cell epitopes are broadly distributed throughout SARS-CoV-2 genome (Ferretti et al., 2020; Tarke et al., 2021a), and the estimated numbers of epitopes per individual are at least 17 for $CD8^+$ T and 19 for $CD4^+$ T cells, respectively

(Tarke et al., 2021a), and thus functional T cell evasion by VOCs is very limited (Tarke et al., 2021b). This in turn suggests that MHC-I downregulation may be a more efficient way for viruses to avoid CTL surveillance than introducing mutations in epitopes, a process that appears to be maximally present in the ancestral SARS-CoV-2 lineage. The importance of MHC-I evasion by SARS-CoV-2 is also highlighted by the fact that no genetic mutations or variations in the MHC-I pathway has thus far been identified as a risk factor for severe COVID (COVID-19 Host Genetics Initiative, 2021), unlike innate immune pathways involving TLRs and type I IFNs (Zhang et al., 2022).

SARS-CoV-2 infection in both human and preclinical models have shown to induce antigen-specific $CD8^+$ T cell responses (Grifoni et al., 2021; Joag et al., 2021), and the early CTL response correlated with a milder disease outcome in human (Tan et al., 2021). Adoptive transfer of serum or IgG from convalescent animals alone, however, is enough to reduce viral load in recipients after SARS-CoV-2 challenge in mice and non-human primates (Israelow et al., 2021; McMahan et al., 2021) and neutralizing antibody is shown to be a strong correlate of protection (Earle et al., 2021; Israelow et al., 2021; Khoury et al., 2021). The protective roles of $CD8^+$ T cell-mediated immunity appear to be more important in

the absence of the optimal humoral responses/neutralizing antibody (Bange et al., 2021; Israelow et al., 2021). Blood anti-ORF8 antibodies can be used as the highly sensitive clinical marker for SARS-CoV-2 infection early (~14 days) after symptom onset (Hachim et al., 2020; Wang et al., 2020), which suggests the role of ORF8 in the very early stage of the disease. ORF8-mediated MHC-I downregulation can therefore precede antigen presentation and hinder priming of viral antigen-specific $CD8^+$ T cell immune responses. Robust MHC-I shutdown by SARS-CoV-2 may explain in part the less effective protection by $CD8^+$ T cells and the less impact of $CD8^+$ T cell absence compared with humoral immunity (Israelow et al., 2021).

Collectively, our data shed light on the intrinsically potent ability of SARS-CoV-2 to avoid the MHC-I mediated antigen presentation to $CD8^+$ T cells. Importantly, we observed a complete inhibition of MHC-I upregulation in lung epithelial cells infected with SARS-CoV-2 at the early stage of infection in a mouse model. Since the ability of ORF8 to downregulate MHC-I is a newly acquired feature in SARS-CoV-2 ORF8 and is absent in SARS-CoV ORF8 (Zhang et al., 2021), it is possible that ORF8 played a role in the efficient replication and transmission of SARS-CoV-2 in human and contributed to its

pandemic potential. Our work provides insights into SARS-CoV-2 pathogenesis and evolution and predicts difficulty for CD8 T cell-based therapeutic approaches to COVID-19.

EXPERIMENTAL MODEL AND SUBJECT DETAILS

Mice

Six to ten-week-old male C57BL6 mice were purchased from the Jackson Laboratory. All animal experiments in this study complied with federal and institutional policies of the Yale Animal Care and Use Committee.

Cell lines and viruses

HEK293T cells were maintained in DMEM supplemented with 1% Penicillin-Streptomycin and 10% heat-inactivated FBS. Calu-3 cells were maintained in MEM supplemented with 1% Penicillin-Streptomycin and 10% heat-inactivated FBS. TMPRSS2-VeroE6 cells were maintained in DMEM supplemented with 1% sodium pyruvate, 1% Penicillin-Streptomycin and 10% heat-inactivated FBS at 37C. Influenza virus A/Puerto Rico/8/34 was kindly provided by Dr. Hideki Hasegawa (National Institute of Infectious Diseases in Japan). Virus stocks were propagated in allantoic cavities from 10- to 11-day-old fertile chicken eggs for 2 days at 35C. Viral titers were determined by standard plaque assay procedure. SARS-CoV-2 MA10 (Leist et al., 2020) was kindly provided by Dr. Ralph S. Baric (University of North Carolina at Chapel Hill). SARS-CoV-2 lineage A (USA-

WA1/2020) and B.1.351b (hCoV-19/South Africa/KRISP-K005325/2020) were obtained from BEI resources. B.1.1.7, B.1.351a, P.1, B.1.617.2, B.1.427, B.1.429, and B.1.526 lineages were isolated and sequenced as part of the Yale Genomic Surveillance Initiative's weekly surveillance program in Connecticut, United States. Virus stocks were propagated and titered as previously described (Lucas et al., 2021; Perez-Then et al., 2022). Briefly, TMPRSS2-VeroE6 cells were infected at multiplicity of infection of 0.01 for 3 days and the cell-free supernatant was collected and used as working stocks. All experiments using live SARS-CoV-2 were performed in a biosafety level 3 laboratory with approval from the Yale Environmental Health and Safety office.

METHOD DETAILS

Viral genome sequence analysis

SARS-CoV-2 variant genome sequences (3,067 sequences) were downloaded from GISAID database (https://www.gisaid.org/) as of February 23, 2022. Sequences of Wuhan Hu-1 (GenBank accession: NC_045512.2) and USA-WA1/2020 (GenBank accession: MW811435.1) were obtained from NCBI Virus SARS-CoV-2 Data Hub (https://www.ncbi.nlm.nih.gov/labs/virus/vssi/#/sars-cov-

2). To investigate the prevalence of amino acid mutations, we downloaded up to 965 sequences of each lineage and aligned the ORF8 nucleotide sequences using Jalview software (http://www.jalview.org/) (Waterhouse et al. Bioinformatics. 2009) by MUSCLE algorithm (Edgar RC. Nucleic Acid Res. 2004). Sequences containing undetermined nucleotides within the codon of interest were removed for analysis. ORF8 amino acid sequence alignment was conducted by Jalview software using MUSCLE algorithm.

Viral infection

Mice were fully anesthetized by intraperitoneal injection of ketamine and xylazine, and intranasally inoculated with 50ul of PBS containing $1x10^5$ PFU of influenza virus A/Puerto Rico/8/34. For SARS-CoV-2 infection in the animal biosafety level 3 facility, mice were anesthetized by 30% v/v isoflurane diluted in propylene glycol, and 50ul of $1x10^5$ PFU of SARS-CoV-2 MA10 in PBS was intranasally delivered. For cell culture infection, cells were washed with PBS and infected with SARS-CoV-2 at a multiplicity of infection of 0.01 or 0.3 for 1 h at 37C. After 1 h incubation, cells were supplemented with complete media and cultured until sample harvest.

Plasmids

pDONR207-SARS-CoV-2 E (#141273), pDONR207-SARS-CoV-2 M (#141274), pDONR207-SARS-CoV-2 ORF7a (#141276), pDONR223-SARS-CoV-2 ORF7b (#141277), pDONR223-SARS-CoV-2 ORF8 (#141278) were purchased from addgene (Kim et al., 2020) and used as templates for construction of plasmids expressing SARS-CoV-2 viral proteins. For HIV Nef expressing plasmid construction, NL4-3-dE-EGFP (kindly provided by Dr. Ya-Chi Ho) was used as a template. The full-length viral genes were amplified by PCR using iProof™ High-Fidelity DNA Polymerase (Bio-Rad), with templates described above and specific primers containing XhoI (XbaI for HIV Nef) and BamHI sites at the 5' and 3' ends, respectively. Following restriction enzyme digestion, PCR fragments were cloned into c-Flag pcDNA3 vector (addgene, #20011).

For construction of plasmids expressing SARS-CoV viral proteins, oligonucleotides corresponding to both strands of SARS-CoV Tor2 (GenBank accession: NC_004718.3) ORF8a and ORF8b containing XhoI and BamHI sites at the 5' and 3' ends were synthesized (IDT) and cloned into XhoI-BamHI site of c-Flag pcDNA3 vector.

Mutant SARS-CoV-2 ORF8 expressing plasmids were generated by standard

PCR-based mutagenesis method. Integrity of inserts was verified by sequencing (Yale Keck DNA sequencing facility).

Lung cell isolation

Lungs were harvested and processed as previously described (Israelow et al., 2021). In Brief, lungs were minced with scissors and digested in RPMI1640 media containing 1mg/ml collagenase A, 30ug/ml DNase I at 37C for 45 min. Digested lungs were then filtered through 70um cell strainer and treated with ACK buffer for 2 min. After washing with PBS, cells were resuspended in PBS with 1% FBS.

Flow cytometry

Cells were blocked with Human BD Fc Block (Fc1.3216, 1:100, BD Biosciences) in the presence of Live/Dead Fixable Aqua (Thermo Fisher) for 15 min at room temperature. Staining antibodies were added and incubated for 20 min at room temperature. Cells were washed with 2mM EDTA-PBS and resuspended in 100ul 2% PFA for 1 hour at room temperature. For intracellular staining, PFA-fixed cells were washed and permeabilized with eBioscience FoxP3/Transcription Factor Staining Buffer (Thermo Fisher) for 10min at 4C. Cells were washed once and

stained in the same permeabilization buffer containing staining antibodies. After 30min incubation at 4C, cells were washed and resuspended in PBS with 1% FBS for analysis on Attune NxT (Thermo Fisher). FlowJo software (Tree Star) was used for the data analysis. Staining antibodies are as follows (Hu Fc Block Pure Fc1.3216 (BD, Cat# 564220), APC anti-HLA-ABC (Thermofisher, Cat# 17-9983-42), APC/Cy7 anti-HLA-DR (BioLegend, Cat# 307618), PE anti-DYKDDDDK Tag (BioLegend, Cat# 637309), AF488 anti-SARS-CoV-2 Spike S1 Subunit (R&D Systems,Cat# FAB105403G), FITC anti-Influenza A NP (Thermofisher, Cat# MA1-7322), PE anti-mouse CD45 (BioLegend, Cat# 109808), BV421 anti-mouse CD31 (BioLegend, Cat# 102423), APC anti-mouse EpCAM (BioLegend, Cat# 118213), PerCP/Cy5.5 anti-H-2Kb/H-2Db (BioLegend,Cat# 114620)).

Quantitative PCR

SARS-CoV-2 infected cells were washed with PBS and lysed with TRIzol reagent (Invitrogen). Total RNA was extracted using RNeasy mini kit (QIAGEN) and reverse transcribed into cDNA using iScript cDNA synthesis kit (Bio-Rad). RT-PCR was performed by CFX96 Touch Real-Time PCR detection system (Bio-

Rad) using iTaq SYBR premix (Bio-Rad) and following primers (5'-3'): HLA-A (Forward: AAAAGGAGGGAGTTACACTCAGG, Reverse: GCTGTGAGGGACAC ATCAGAG), HLA-B (Forward: CTACCCTGCGGAGATCA, Reverse: ACAGCCA GGCCAGCAACA), HLA-C (Forward: CACACCTCTCCTTTGTGACTTCAA, Reverse: CCACCTCCTCACATTATGCTAACA), human ISG15 (Forward: TGGAC AAATGCGACGAACCTC, Reverse: TCAGCCGTACCTCGTAGGTG), human ISG20 (Forward: TCTACGACACGTCCACTGACA, Reverse: CTGTTCTGGATG CTCTTGTGT), human OAS1 (Forward: CTGAGAAGGCAGCTCACGAA, Reverse: TGTGCTGGGTCAGCAGAATC), human GAPDH (Forward: CAACGG ATTTGGTCGTATT, Reverse: GATGGCAACAATATCCACTT),.

Statistical analysis

Statistical significance was tested using one-way analysis of variance (ANOVA) with Tukey's multiple comparison test. P-values of <0.05 were considered statistically significant.

Acknowledgement:

We thank Melissa Linehan and Huiping Dong for technical and logistical assistance. We thank Ralph Baric for kindly providing SASR-CoV-2 MA10. We thank Ya-Chi Ho for kindly providing NL4-3-dE-EGFP. We thank Craig Wilen for his technical expertise. We thank

Benjamin Israelow and Tianyang Mao for critical reading of the manuscript. We also give special recognition to the services of Ben Fontes and the Yale EH&S Department for their ongoing assistance in safely conducting biosafety level 3 research. This work was in part supported by the Fast Grant from Emergent Ventures at the Mercatus Center and 1R01AI157488. A.I. is an Investigator of the Howard Hughes Medical Institute. M.M. is supported by the Japan Society for Promotion of Science Overseas fellowship.

Author contributions:

M.M., C.L., and A.I. conceived of and designed the project. M.M., C.L., and V.M. performed experiments. M.M., C.L., and V.M. analyzed and interpreted data. M.M. and A.I. wrote the manuscript and all authors reviewed and provided feedback on the manuscript.

Competing interests:

Authors declare no competing interest.

Corresponding authors:

Correspondence and requests for materials should be addressed to A.I.

References

Agerer, B., Koblischke, M., Gudipati, V., Montano-Gutierrez, L.F., Smyth, M., Popa, A., Genger, J.W., Endler, L., Florian, D.M., Muhlgrabner, V.*, et al.* (2021). SARS-CoV-2 mutations in MHC-I-restricted epitopes evade CD8(+) T cell responses. Sci Immunol *6*.

Alkhansa, A., Lakkis, G., and El Zein, L. (2021). Mutational analysis of SARS-CoV-2 ORF8 during six months of COVID-19 pandemic. Gene Rep *23*, 101024.

Bange, E.M., Han, N.A., Wileyto, P., Kim, J.Y., Gouma, S., Robinson, J., Greenplate, A.R., Hwee, M.A., Porterfield, F., Owoyemi, O.*, et al.* (2021). CD8(+) T cells contribute to survival in patients with COVID-19 and hematologic cancer. Nat Med *27*, 1280-1289.

Ceraolo, C., and Giorgi, F.M. (2020). Genomic variance of the 2019-nCoV coronavirus. J Med Virol *92*, 522-528.

Consortium, C.S.M.E. (2004). Molecular evolution of the SARS coronavirus during the course of the SARS epidemic in China. Science *303*, 1666-1669.

Cui, J., Li, F., and Shi, Z.L. (2019). Origin and evolution of pathogenic coronaviruses. Nat Rev Microbiol *17*, 181-192.

Earle, K.A., Ambrosino, D.M., Fiore-Gartland, A., Goldblatt, D., Gilbert, P.B., Siber, G.R., Dull, P., and Plotkin, S.A. (2021). Evidence for antibody as a protective correlate for COVID-19 vaccines. Vaccine *39*, 4423-4428.

Ferretti, A.P., Kula, T., Wang, Y., Nguyen, D.M.V., Weinheimer, A., Dunlap, G.S., Xu, Q., Nabilsi, N., Perullo, C.R., Cristofaro, A.W.*, et al.* (2020). Unbiased Screens Show CD8(+) T Cells of COVID-19 Patients Recognize Shared Epitopes in SARS-CoV-2 that Largely Reside outside the Spike Protein. Immunity *53*, 1095-1107 e1093.

Fong, S.W., Yeo, N.K., Chan, Y.H., Goh, Y.S., Amrun, S.N., Ang, N., Rajapakse, M.P., Lum, J., Foo, S., Lee, C.Y.*, et al.* (2022). Robust Virus-Specific Adaptive Immunity in COVID-19 Patients with SARS-CoV-2 Delta382 Variant Infection. J Clin Immunol *42*, 214-229.

Garcia-Beltran, W.F., Lam, E.C., St Denis, K., Nitido, A.D., Garcia, Z.H., Hauser, B.M., Feldman, J., Pavlovic, M.N., Gregory, D.J., Poznansky, M.C.*, et al.* (2021). Multiple SARS-CoV-2 variants escape neutralization by vaccine-induced humoral immunity. Cell *184*, 2523.

Geng, H., Subramanian, S., Wu, L., Bu, H.F., Wang, X., Du, C., De Plaen, I.G., and Tan, X.D. (2021). SARS-CoV-2 ORF8 Forms Intracellular Aggregates and Inhibits IFNgamma-Induced Antiviral Gene Expression in Human Lung Epithelial Cells. Front Immunol *12*, 679482.

Grifoni, A., Sidney, J., Vita, R., Peters, B., Crotty, S., Weiskopf, D., and Sette, A. (2021). SARS-CoV-2 human T cell epitopes: Adaptive immune response against COVID-19. Cell Host Microbe *29*, 1076-1092.

Guan, Y., Zheng, B.J., He, Y.Q., Liu, X.L., Zhuang, Z.X., Cheung, C.L., Luo, S.W., Li, P.H.,

Zhang, L.J., Guan, Y.J., *et al.* (2003). Isolation and characterization of viruses related to the SARS coronavirus from animals in southern China. Science *302*, 276-278.

Guo, K., Barrett, B.S., Mickens, K.L., Vladar, E.K., Morrison, J.H., Hasenkrug, K.J., Poeschla, E.M., and Santiago, M.L. (2021). Interferon Resistance of Emerging SARS-CoV-2 Variants. bioRxiv.

Habel, J.R., Nguyen, T.H.O., van de Sandt, C.E., Juno, J.A., Chaurasia, P., Wragg, K., Koutsakos, M., Hensen, L., Jia, X., Chua, B., *et al.* (2020). Suboptimal SARS-CoV-2-specific CD8(+) T cell response associated with the prominent HLA-A*02:01 phenotype. Proc Natl Acad Sci U S A *117*, 24384-24391.

Hachim, A., Kavian, N., Cohen, C.A., Chin, A.W.H., Chu, D.K.W., Mok, C.K.P., Tsang, O.T.Y., Yeung, Y.C., Perera, R., Poon, L.L.M., *et al.* (2020). ORF8 and ORF3b antibodies are accurate serological markers of early and late SARS-CoV-2 infection. Nat Immunol *21*, 1293-1301.

Hansen, T.H., and Bouvier, M. (2009). MHC class I antigen presentation: learning from viral evasion strategies. Nat Rev Immunol *9*, 503-513.

Hu, B., Zeng, L.P., Yang, X.L., Ge, X.Y., Zhang, W., Li, B., Xie, J.Z., Shen, X.R., Zhang, Y.Z., Wang, N., *et al.* (2017). Discovery of a rich gene pool of bat SARS-related coronaviruses provides new insights into the origin of SARS coronavirus. PLoS Pathog *13*, e1006698.

Initiative, C.-H.G. (2021). Mapping the human genetic architecture of COVID-19. Nature *600*, 472-477.

Israelow, B., Mao, T., Klein, J., Song, E., Menasche, B., Omer, S.B., and Iwasaki, A. (2021). Adaptive immune determinants of viral clearance and protection in mouse models of SARS-CoV-2. Sci Immunol *6*, eabl4509.

Joag, V., Wijeyesinghe, S., Stolley, J.M., Quarnstrom, C.F., Dileepan, T., Soerens, A.G., Sangala, J.A., O'Flanagan, S.D., Gavil, N.V., Hong, S.W., *et al.* (2021). Cutting Edge: Mouse SARS-CoV-2 Epitope Reveals Infection and Vaccine-Elicited CD8 T Cell Responses. J Immunol *206*, 931-935.

Khoury, D.S., Cromer, D., Reynaldi, A., Schlub, T.E., Wheatley, A.K., Juno, J.A., Subbarao, K., Kent, S.J., Triccas, J.A., and Davenport, M.P. (2021). Neutralizing antibody levels are highly predictive of immune protection from symptomatic SARS-CoV-2 infection. Nat Med *27*, 1205-1211.

Kim, D.K., Knapp, J.J., Kuang, D., Chawla, A., Cassonnet, P., Lee, H., Sheykhkarimli, D., Samavarchi-Tehrani, P., Abdouni, H., Rayhan, A., *et al.* (2020). A Comprehensive, Flexible Collection of SARS-CoV-2 Coding Regions. G3 (Bethesda) *10*, 3399-3402.

Kriplani, N., Clohisey, S., Fonseca, S., Fletcher, S., Lee, H., M., Ashworth, J., Kurian, D., Lycett, S., J., Tait-Burkard, C., Baillie, J., K., *et al.* (2021). Secreted SARS-CoV-2 ORF8

modulates the cytokine expression profile of human macrophages. bioRxiv.

Kustin, T., Harel, N., Finkel, U., Perchik, S., Harari, S., Tahor, M., Caspi, I., Levy, R., Leshchinsky, M., Ken Dror, S.*, et al.* (2021). Evidence for increased breakthrough rates of SARS-CoV-2 variants of concern in BNT162b2-mRNA-vaccinated individuals. Nat Med *27*, 1379-1384.

Lei, X., Dong, X., Ma, R., Wang, W., Xiao, X., Tian, Z., Wang, C., Wang, Y., Li, L., Ren, L.*, et al.* (2020). Activation and evasion of type I interferon responses by SARS-CoV-2. Nat Commun *11*, 3810.

Leist, S.R., Dinnon, K.H., 3rd, Schafer, A., Tse, L.V., Okuda, K., Hou, Y.J., West, A., Edwards, C.E., Sanders, W., Fritch, E.J.*, et al.* (2020). A Mouse-Adapted SARS-CoV-2 Induces Acute Lung Injury and Mortality in Standard Laboratory Mice. Cell *183*, 1070-1085 e1012.

Li, J.Y., Liao, C.H., Wang, Q., Tan, Y.J., Luo, R., Qiu, Y., and Ge, X.Y. (2020). The ORF6, ORF8 and nucleocapsid proteins of SARS-CoV-2 inhibit type I interferon signaling pathway. Virus Res *286*, 198074.

Lucas, C., Vogels, C.B.F., Yildirim, I., Rothman, J.E., Lu, P., Monteiro, V., Gehlhausen, J.R., Campbell, M., Silva, J., Tabachnikova, A.*, et al.* (2021). Impact of circulating SARS-CoV-2 variants on mRNA vaccine-induced immunity. Nature *600*, 523-529.

McMahan, K., Yu, J., Mercado, N.B., Loos, C., Tostanoski, L.H., Chandrashekar, A., Liu, J., Peter, L., Atyeo, C., Zhu, A.*, et al.* (2021). Correlates of protection against SARS-CoV-2 in rhesus macaques. Nature *590*, 630-634.

Motozono, C., Toyoda, M., Zahradnik, J., Saito, A., Nasser, H., Tan, T.S., Ngare, I., Kimura, I., Uriu, K., Kosugi, Y.*, et al.* (2021). SARS-CoV-2 spike L452R variant evades cellular immunity and increases infectivity. Cell Host Microbe *29*, 1124-1136 e1111.

Perez-Then, E., Lucas, C., Monteiro, V.S., Miric, M., Brache, V., Cochon, L., Vogels, C.B.F., Malik, A.A., De la Cruz, E., Jorge, A.*, et al.* (2022). Neutralizing antibodies against the SARS-CoV-2 Delta and Omicron variants following heterologous CoronaVac plus BNT162b2 booster vaccination. Nat Med *28*, 481-485.

Planas, D., Saunders, N., Maes, P., Guivel-Benhassine, F., Planchais, C., Buchrieser, J., Bolland, W.H., Porrot, F., Staropoli, I., Lemoine, F.*, et al.* (2022). Considerable escape of SARS-CoV-2 Omicron to antibody neutralization. Nature *602*, 671-675.

Sabino, E.C., Buss, L.F., Carvalho, M.P.S., Prete, C.A., Jr., Crispim, M.A.E., Fraiji, N.A., Pereira, R.H.M., Parag, K.V., da Silva Peixoto, P., Kraemer, M.U.G.*, et al.* (2021). Resurgence of COVID-19 in Manaus, Brazil, despite high seroprevalence. Lancet *397*, 452-455.

Schwartz, O., Marechal, V., Le Gall, S., Lemonnier, F., and Heard, J.M. (1996). Endocytosis of major histocompatibility complex class I molecules is induced by the HIV-1 Nef protein.

Nat Med *2*, 338-342.

Stumptner-Cuvelette, P., Morchoisne, S., Dugast, M., Le Gall, S., Raposo, G., Schwartz, O., and Benaroch, P. (2001). HIV-1 Nef impairs MHC class II antigen presentation and surface expression. Proc Natl Acad Sci U S A *98*, 12144-12149.

Su, Y.C.F., Anderson, D.E., Young, B.E., Linster, M., Zhu, F., Jayakumar, J., Zhuang, Y., Kalimuddin, S., Low, J.G.H., Tan, C.W.*, et al.* (2020). Discovery and Genomic Characterization of a 382-Nucleotide Deletion in ORF7b and ORF8 during the Early Evolution of SARS-CoV-2. mBio *11*.

Tan, A.T., Linster, M., Tan, C.W., Le Bert, N., Chia, W.N., Kunasegaran, K., Zhuang, Y., Tham, C.Y.L., Chia, A., Smith, G.J.D.*, et al.* (2021). Early induction of functional SARS-CoV-2-specific T cells associates with rapid viral clearance and mild disease in COVID-19 patients. Cell Rep *34*, 108728.

Tao, K., Tzou, P.L., Nouhin, J., Gupta, R.K., de Oliveira, T., Kosakovsky Pond, S.L., Fera, D., and Shafer, R.W. (2021). The biological and clinical significance of emerging SARS-CoV-2 variants. Nat Rev Genet *22*, 757-773.

Tarke, A., Sidney, J., Kidd, C.K., Dan, J.M., Ramirez, S.I., Yu, E.D., Mateus, J., da Silva Antunes, R., Moore, E., Rubiro, P.*, et al.* (2021a). Comprehensive analysis of T cell immunodominance and immunoprevalence of SARS-CoV-2 epitopes in COVID-19 cases. Cell Rep Med *2*, 100204.

Tarke, A., Sidney, J., Methot, N., Yu, E.D., Zhang, Y., Dan, J.M., Goodwin, B., Rubiro, P., Sutherland, A., Wang, E.*, et al.* (2021b). Impact of SARS-CoV-2 variants on the total CD4(+) and CD8(+) T cell reactivity in infected or vaccinated individuals. Cell Rep Med *2*, 100355.

Thorne, L.G., Bouhaddou, M., Reuschl, A.K., Zuliani-Alvarez, L., Polacco, B., Pelin, A., Batra, J., Whelan, M.V.X., Hosmillo, M., Fossati, A.*, et al.* (2022). Evolution of enhanced innate immune evasion by SARS-CoV-2. Nature *602*, 487-495.

Velazquez-Salinas, L., Zarate, S., Eberl, S., Gladue, D.P., Novella, I., and Borca, M.V. (2020). Positive Selection of ORF1ab, ORF3a, and ORF8 Genes Drives the Early Evolutionary Trends of SARS-CoV-2 During the 2020 COVID-19 Pandemic. Front Microbiol *11*, 550674.

Wang, P., Nair, M.S., Liu, L., Iketani, S., Luo, Y., Guo, Y., Wang, M., Yu, J., Zhang, B., Kwong, P.D.*, et al.* (2021). Antibody resistance of SARS-CoV-2 variants B.1.351 and B.1.1.7. Nature *593*, 130-135.

Wang, X., Lam, J.Y., Wong, W.M., Yuen, C.K., Cai, J.P., Au, S.W., Chan, J.F., To, K.K.W., Kok, K.H., and Yuen, K.Y. (2020). Accurate Diagnosis of COVID-19 by a Novel Immunogenic Secreted SARS-CoV-2 orf8 Protein. mBio *11*.

Yoo, J.S., Sasaki, M., Cho, S.X., Kasuga, Y., Zhu, B., Ouda, R., Orba, Y., de Figueiredo, P., Sawa, H., and Kobayashi, K.S. (2021). SARS-CoV-2 inhibits induction of the MHC class I

pathway by targeting the STAT1-IRF1-NLRC5 axis. Nat Commun *12*, 6602.

Young, B.E., Fong, S.W., Chan, Y.H., Mak, T.M., Ang, L.W., Anderson, D.E., Lee, C.Y., Amrun, S.N., Lee, B., Goh, Y.S.*, et al.* (2020). Effects of a major deletion in the SARS-CoV-2 genome on the severity of infection and the inflammatory response: an observational cohort study. Lancet *396*, 603-611.

Zhang, Q., Bastard, P., Effort, C.H.G., Cobat, A., and Casanova, J.L. (2022). Human genetic and immunological determinants of critical COVID-19 pneumonia. Nature *603*, 587-598.

Zhang, Y., Chen, Y., Li, Y., Huang, F., Luo, B., Yuan, Y., Xia, B., Ma, X., Yang, T., Yu, F.*, et al.* (2021). The ORF8 protein of SARS-CoV-2 mediates immune evasion through down-regulating MHC-Iota. Proc Natl Acad Sci U S A *118*.

Figure regends:

Fig. 1. MHC-I evasion by SARS-CoV-2 variants

(A) Calu-3 cells were infected with SARS-CoV-2 variants at MOI 0.3 for 40h. The cell surface expression of HLA-ABC was analyzed by FACS. (B) Calu-3 cells were infected with SARS-CoV-2 variants at MOI 0.01 for 48h. The mRNA levels of HLA-A, B, and C were measured by RT-qPCR. Data are mean ± s.d. Data are representative of two to three independent experiments. *, $p<0.05$; **, $p< 0.01$; ***, $p< 0.001$

Fig. 2. Unique mutations are found in ORF8 gene of SARS-CoV-2 variants

(A) Mutant proportion in the ORF8 genes of the indicated SARS-CoV-2 variants. The amino acid positions shown are selected based on the results of multiple sequence alignment performed in Fig.S1. The number of sequences analyzed for each lineage is shown above each graph. (B) Frequency of amino acids at the positions enriched for mutants in each variant. The amino acids shown in gray color correspond to WT. (C) Schematic diagram of ORF8 proteins from SARS-CoV-2 variants. (D and E) HEK293T cells were transfected with plasmids encoding C-terminally Flag-tagged SARS-CoV ORF8a/b, SARS-CoV-2 ORF8 WT, or SARS-CoV-2 ORF8 variants. Forty-eight hours after transfection, cells were collected and analyzed for the cell surface HLA-ABC expression. Data are shown in raw MFI (D) or as the ratio of MFI in Flag+ cells to Flag- cells normalized to the value of SARS-CoV ORF8a (E) (n=3). Data are mean ± s.d. Data are representative of three independent experiments. ***, $p< 0.001$

Fig. 3. Impaired interferon-stimulated gene expression by SARS-CoV-2 variants

Calu-3 cells were infected with SARS-CoV-2 variants at MOI 0.01 for 48h. The mRNA levels of ISG15, ISG20, OAS1 were measured by RT-qPCR. Data are mean ± s.d. Data are representative of two independent experiments. * shown in blue is comparison with WA1. *, $p<0.05$; **, $p< 0.01$; ***, $p< 0.001$

Fig. 4. SARS-CoV-2 viral genes redundantly downregulate MHC-I

(A-C) HEK293T cells were transfected with expression plasmids encoding C-terminal Flag-tagged viral proteins as indicated. After 48 hours, surface expressions of HLA-ABC and HLA-DR were analyzed by flow cytometry. The representative histogram of HLA-ABC (A) and HLA-DR (B) of SARS-CoV ORF8a-

Flag, HIV-Nef-Flag, or SARS-CoV-2 ORF8-Flag +/- cells are shown. (C) The normalized ratio of HLA surface expression in Flag+ cells to Flag- cells are shown (n=3). Data are mean ± s.d. Data are representative of three independent experiments. Statistical significance is calculated versus SARS-CoV ORF8a *, p< 0.05; ***, p< 0.001

Fig. 5. Robust suppression of MHC-I upregulation by SARS-CoV-2 *in vivo*

(A-C) C57BL/6J mice were infected intranasally with 10^5 PFU of SARS-CoV-2 MA10 or Influenza virus A/PR8. Two days later, lungs were collected and analyzed for surface MHC-I expressions on epithelial cells of viral protein (SARS-CoV-2 Spike (S) or Influenza A virus Nucleoprotein (NP)) positive and negative populations. (n=3). The representative histograms (A) and MFI (B and C) are shown. Data are mean ± s.e.m. Data are representative of two independent experiments. *, p<0.05; **, p< 0.01; ***, p< 0.001

Fig. S1. Comprehensive screening of mutations in ORF8 in variants of concern/interest

Multiple sequence alignment of ORF8 protein from SARS-CoV-2 variants. Amino acid residues are colored according to ClustalX color scheme by physicochemical properties.

Fig.1

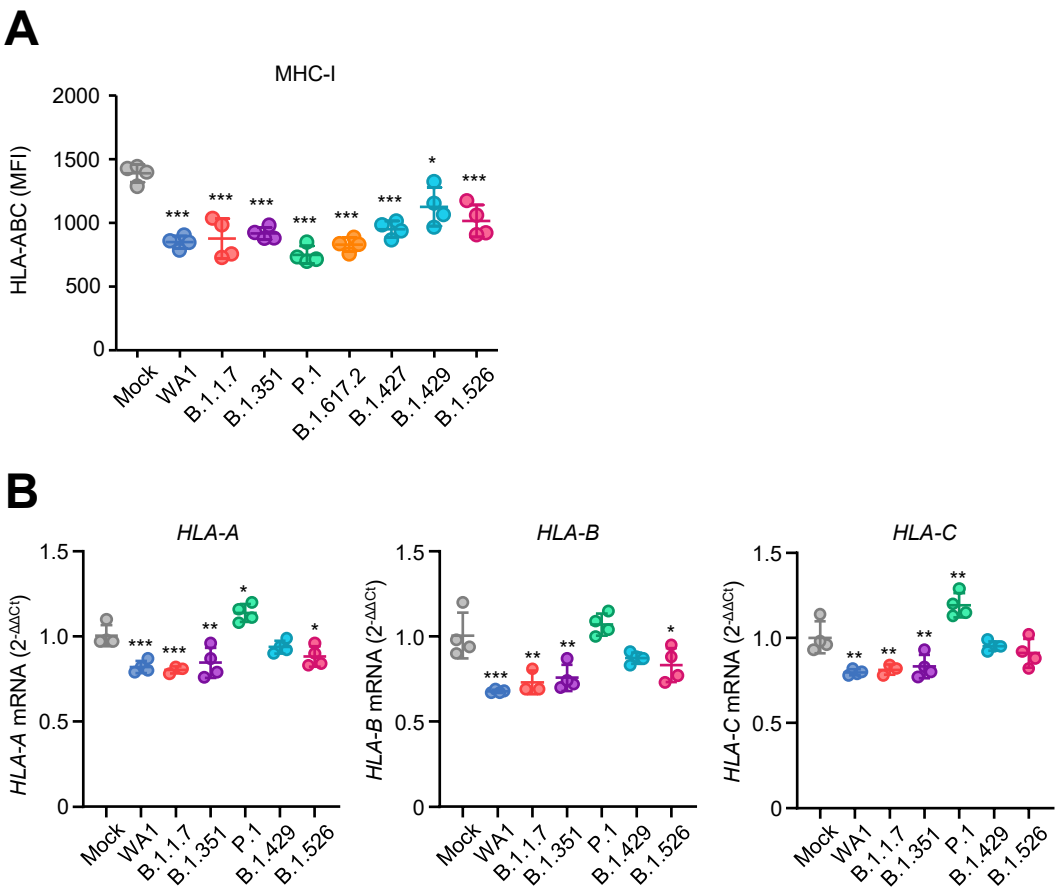
A
MHC-I
HLA-ABC (MFI)
2000
1500
1000
500
0
Mock
WA1
B.1.1.7
B.1.351
P.1
B.1.617.2
B.1.427
B.1.429
B.1.526
B
HLA-A
HLA-B
HLA-C
HLA-A mRNA (2-ΔΔCt)
HLA-B mRNA (2-ΔΔCt)
HLA-C mRNA (2-ΔΔCt)
1.5
1.0
0.5
0

Fig.2

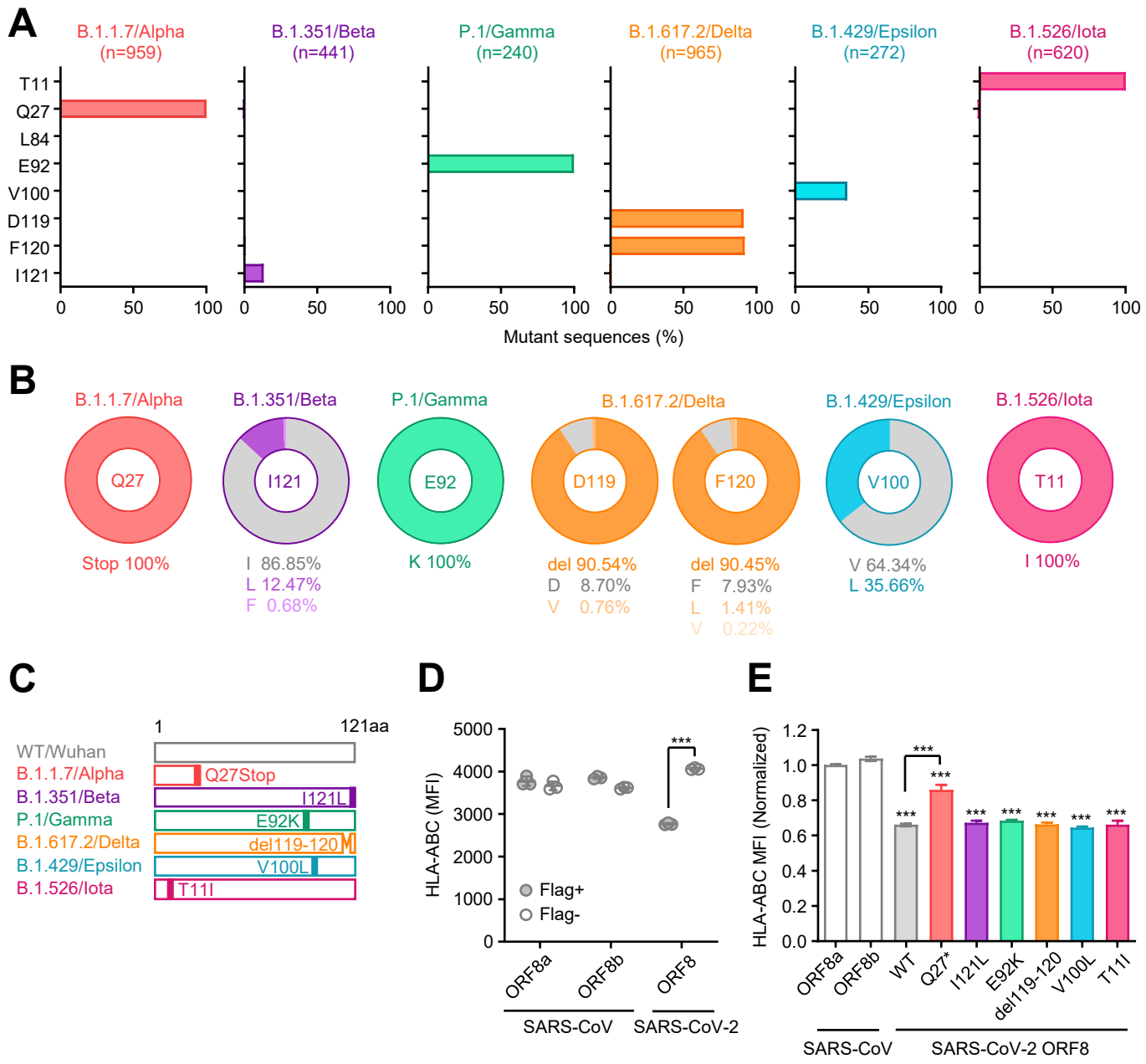
A
B.1.1.7/Alpha (n=959)
B.1.351/Beta (n=441)
P.1/Gamma (n=240)
B.1.617.2/Delta (n=965)
B.1.429/Epsilon (n=272)
B.1.526/Iota (n=620)
T11
Q27
L84
E92
V100
D119
F120
I121
0
50
100
Mutant sequences (%)
B
B.1.1.7/Alpha
Q27
Stop 100%
B.1.351/Beta
I121
I 86.85%
L 12.47%
F 0.68%
P.1/Gamma
E92
K 100%
B.1.617.2/Delta
D119
del 90.54%
D 8.70%
V 0.76%
F120
del 90.45%
F 7.93%
L 1.41%
V 0.22%
B.1.429/Epsilon
V100
V 64.34%
L 35.66%
B.1.526/Iota
T11
I 100%
C
1
121aa
WT/Wuhan
B.1.1.7/Alpha
Q27Stop
B.1.351/Beta
I121L
P.1/Gamma
E92K
B.1.617.2/Delta
del119-120
B.1.429/Epsilon
V100L
B.1.526/Iota
T11I
D
HLA-ABC (MFI)
5000
4000
3000
2000
1000
0
***
Flag+
Flag-
ORF8a
ORF8b
ORF8
SARS-CoV
SARS-CoV-2
E
HLA-ABC MFI (Normalized)
1.2
1.0
0.8
0.6
0.4
0.2
0.0
***
ORF8a
ORF8b
WT
Q27*
I121L
E92K
del119-120
V100L
T11I
SARS-CoV
SARS-CoV-2 ORF8

Fig.3

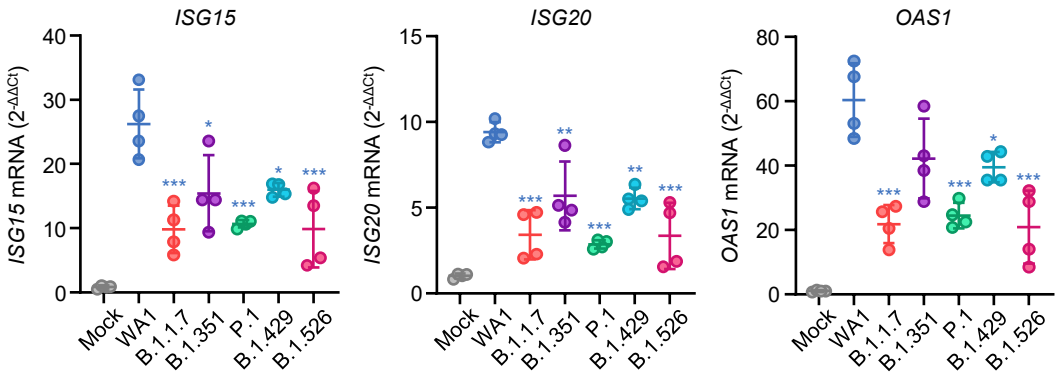
ISG15
ISG15 mRNA (2-ΔΔCt)
40
30
20
10
0
Mock
WA1
B.1.1.7
B.1.351
P.1
B.1.429
B.1.526
ISG20
ISG20 mRNA (2-ΔΔCt)
15
10
5
0
OAS1
OAS1 mRNA (2-ΔΔCt)
80
60
40
20
0

Fig.4

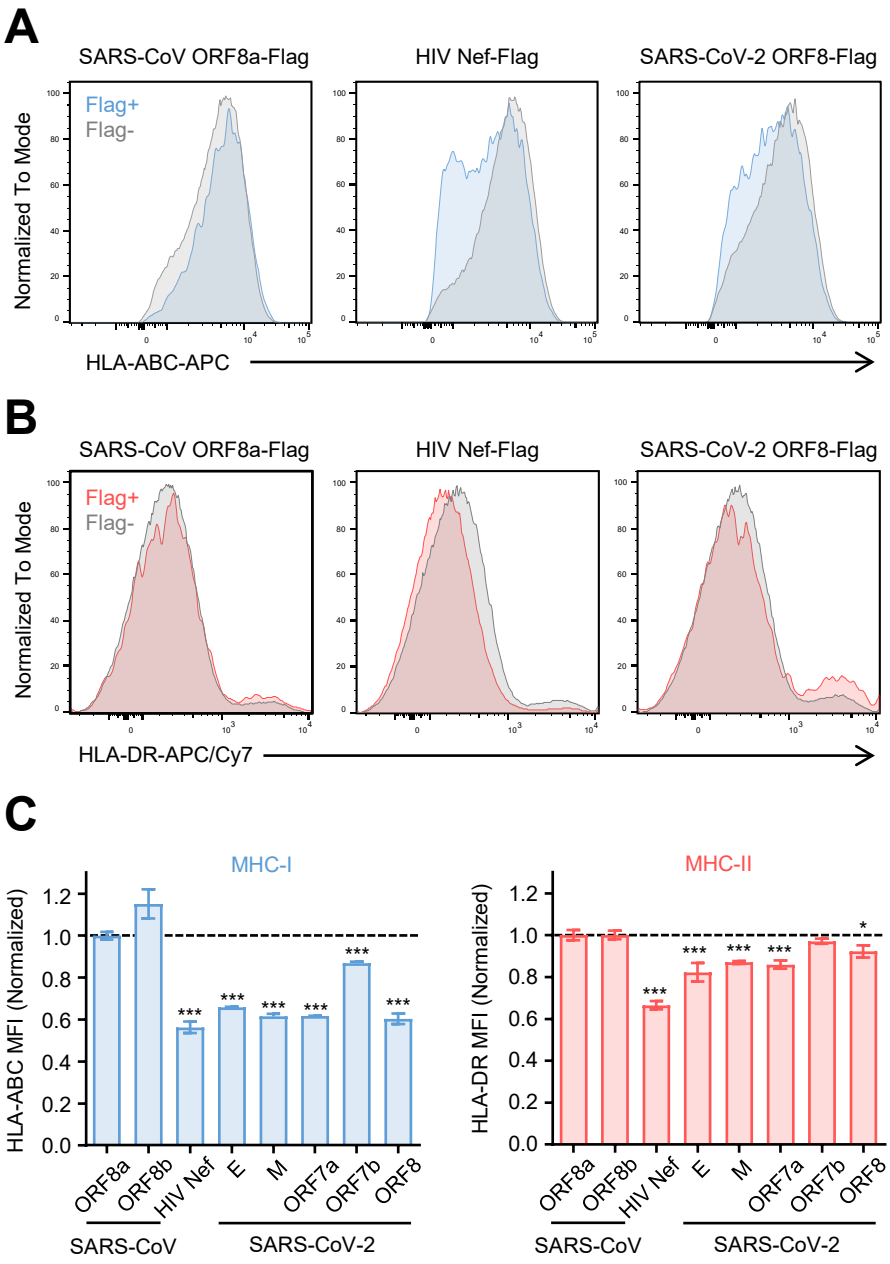
A
SARS-CoV ORF8a-Flag
HIV Nef-Flag
SARS-CoV-2 ORF8-Flag
Flag+
Flag-
Normalized To Mode
HLA-ABC-APC
B
SARS-CoV ORF8a-Flag
HIV Nef-Flag
SARS-CoV-2 ORF8-Flag
Flag+
Flag-
Normalized To Mode
HLA-DR-APC/Cy7
C
MHC-I
HLA-ABC MFI (Normalized)
ORF8a
ORF8b
HIV Nef
E
M
ORF7a
ORF7b
ORF8
SARS-CoV
SARS-CoV-2
MHC-II
HLA-DR MFI (Normalized)
ORF8a
ORF8b
HIV Nef
E
M
ORF7a
ORF7b
ORF8
SARS-CoV
SARS-CoV-2

Fig.5

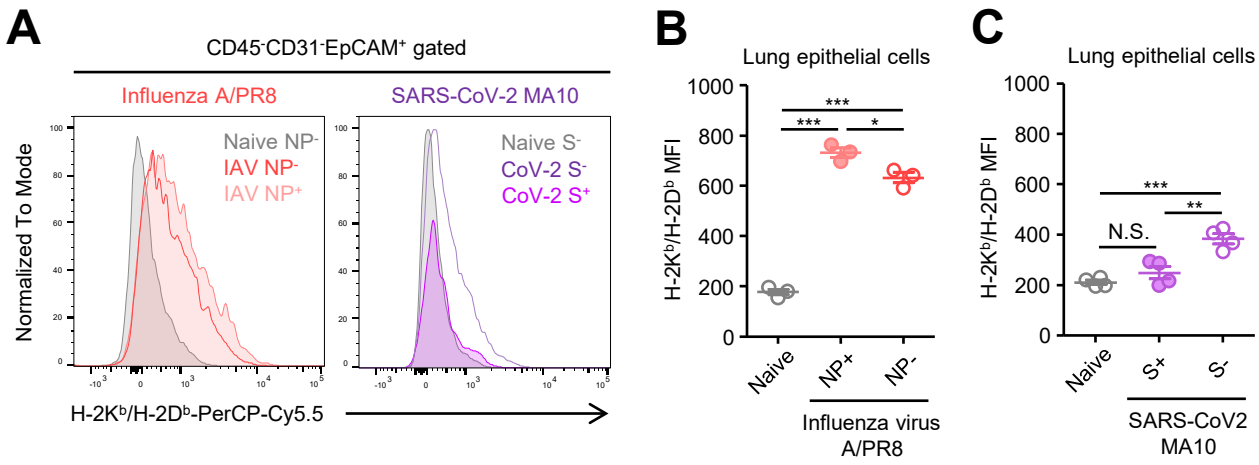
A
CD45-CD31-EpCAM+ gated
Influenza A/PR8
SARS-CoV-2 MA10
Naive NP-
IAV NP-
IAV NP+
Naive S-
CoV-2 S-
CoV-2 S+
Normalized To Mode
H-2Kb/H-2Db-PerCP-Cy5.5
B
Lung epithelial cells
H-2Kb/H-2Db MFI
1000
800
600
400
200
0
***
***
*
Naive
NP+
NP-
Influenza virus A/PR8
C
Lung epithelial cells
H-2Kb/H-2Db MFI
1000
800
600
400
200
0
***
**
N.S.
Naive
S+
S-
SARS-CoV2 MA10

Fig.S1

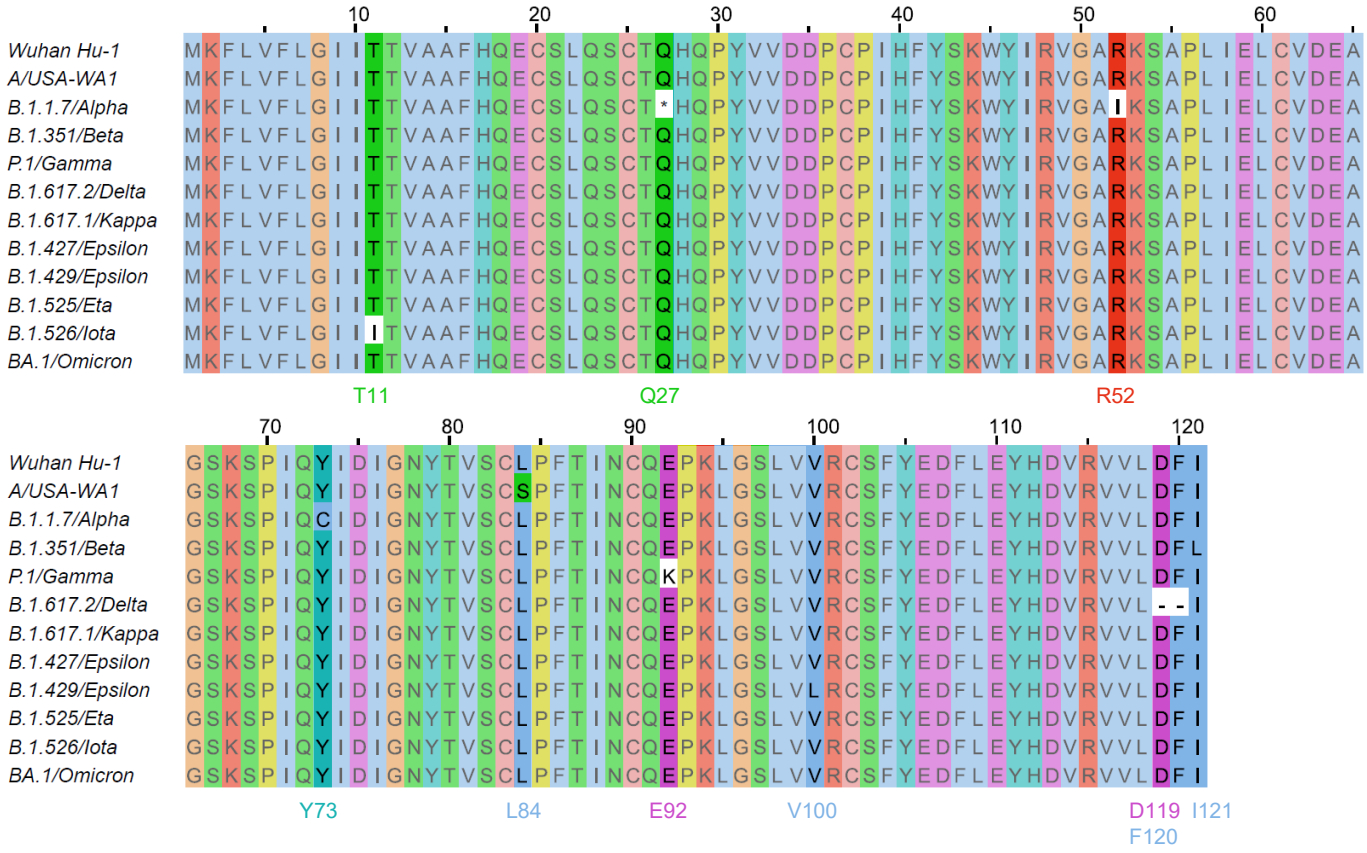
10
20
30
40
50
60
Wuhan Hu-1
A/USA-WA1
B.1.1.7/Alpha
B.1.351/Beta
P.1/Gamma
B.1.617.2/Delta
B.1.617.1/Kappa
B.1.427/Epsilon
B.1.429/Epsilon
B.1.525/Eta
B.1.526/Iota
BA.1/Omicron
T11
Q27
R52
70
80
90
100
110
120
Y73
L84
E92
V100
D119
F120
I121